Phosphoinositide-3-kinase regulatory subunit 4 participates in the occurrence and development of amyotrophic lateral sclerosis by regulating autophagy

From the Contents

Yue Liu[#], Cai-Hui Wei[#], Cheng Li[#], Wen-Zhi Chen[#], Yu Zhu, Ren-Shi Xu[*]

Graphical Abstract *Phosphoinositide-3-kinase regulatory subunit 4 (PIK3R4) possibly inhibits neuronal degeneration to prevent the progression of amyotrophic lateral sclerosis by regulating autophagy*
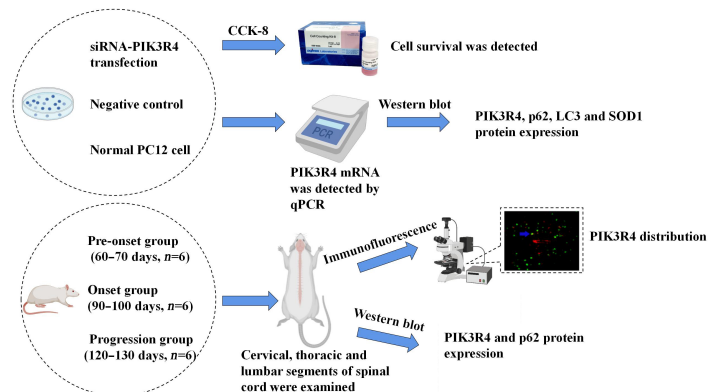
Abstract

The development of amyotrophic lateral sclerosis (ALS) may be related to the abnormal alterations of multiple proteins. Our previous study revealed that the expression of phosphoinositide-3-kinase regulatory subunit 4 (PIK3R4) was decreased in ALS. However, the role of PIK3R4 in ALS pathogenesis remains unknown. This study was the first to find that transfection of PC12 cells with small interfering RNA against the PIK3R4 gene significantly decreased the expression levels of PIK3R4 and the autophagy-related proteins p62 and LC3. Additionally, *in vivo* experiments revealed that the PIK3R4 protein was extensively expressed in the anterior horn, posterior horn, central canal, and areas surrounding the central canal in cervical, thoracic, and lumbar segments of the spinal cord in adult mice. PIK3R4 protein was mainly expressed in the neurons within the spinal lumbar segments. PIK3R4 and p62 expression levels were significantly decreased at both the pre-onset and onset stages of ALS disease in Tg(SOD1*G93A)1Gur mice compared with control mice, but these proteins were markedly increased at the progression stage. LC3 protein expression did not change during progression of ALS. These findings suggest that PIK3R4 likely participates in the prevention of ALS progression. This study was approved by the Ethics Committee for Animal Care and Use of Jiangxi Provincial People's Hospital, Affiliated People's Hospital of Nanchang University (approval No. 2020025) on March 26, 2020.
Key Words: amyotrophic lateral sclerosis; autophagy; LC3; p62; PC12 cell; phosphoinositide-3-kinase regulatory subunit 4; spinal cord; Tg(SOD1*G93A)1Gur mice

Chinese Library Classification No. R456; R741; R651.2

Introduction

Amyotrophic lateral sclerosis (ALS), known as Lou Gehrig's disease in the USA, is a neurological disease that results in damage to the upper and lower motor neurons (Boillée et al., 2006; Cai and Fan, 2013; Tsai et al., 2017; Xu and Yuan, 2021). The motor neuron transmits the physiological message from both the brain and spinal cord to the voluntary muscles in the arms, legs, and other parts of the body. ALS patients gradually lose muscle strength and movement abilities.

Eventually, muscles involved in respiration fail, and ALS patients are unable to breathe without a respirator. In the late period of ALS, the majority of patients die from respiratory failure. ALS usually occurs in adults between the ages of 40 and 60 years with higher morbidity in men; however, the exact pathogenesis of the disease is still unclear. Since the discovery of the involvement of mutant superoxide dismutase 1 (SOD1) in ALS, related proteins, such as TAR DNA binding protein (TDP-43) and FUS RNA binding protein (FUS/TLS), have

Department of Neurology, First Affiliated Hospital of Nanchang Medical College, Jiangxi Provincial People's Hospital, Affiliated People's Hospital of Nanchang University, Nanchang, Jiangxi Province, China
*Correspondence to: Ren-Shi Xu, PhD, xurenshi@nuc.edu.cn.
https://orcid.org/0000-0003-0313-3434 (Ren-Shi Xu)
#These authors contributed equally to this work.

been shown to participate in ALS pathogenesis; however, no abnormal proteins have been discovered that can fully explain the pathogenesis of ALS for the entire course of the disease (Mitchell and Borasio, 2007; Ludolph et al., 2012; Salameh et al., 2015; Chen et al., 2021).

Autophagy is a cellular catabolic pathway, which involves the degradation of proteins, turnover of organelles, and non-selective break-down of cytoplasmic components; it is an evolutionarily conserved and exquisitely regulated bioprocess in eukaryotes (Cheon et al., 2019; Yang et al., 2020). The autophagy process initiates with the generation of autophagosomes, which are reticulated double membranes within the cell that engulf cytoplasmic substances and fuse with lysosomes for subsequent degradation of the phagosomal contents. Autophagy is modulated by extra- or intracellular stress signals, including starvation, growth factor deprivation, and endoplasmic reticulum stress (Guo et al., 2018). Furthermore, autophagy exerts a key role in cellular homeostasis and maintenance of the basic quality of cellular components (Codogno et al., 1997; Guo et al., 2018; Jung et al., 2020).

The phosphoinositide-3-kinase regulatory subunit 4 (PIK3R4) gene is located on chromosome 3q22.1. The human PIK3R4 protein is 1358 amino acids in length and approximately 153 kDa in mass. Components of phosphatidylinositol 3-kinase (PI3K) include PIK3C3 (catalytic subunit) and PIK3R4 (regulatory subunit). Beclin 1 associates with the regulatory/auxiliary subunit and may become a part of PI3K, resulting in the formation of an alternative complex. The alternative complexes comprising a fourth regulatory subunit are PI3KC3-C1 (PI3K complex I), which includes autophagy related 14 (ATG14), and PI3KC3-C2 (PI3K complex II), which includes beclin 1 binding protein (Panaretou et al., 1997; Matsunaga et al., 2009; Fogel et al., 2013; Baskaran et al., 2014). PI3KC3-C1 exhibits a V-shaped architecture with PIK3R4, which serves as the bridge between PIK3C3 and the ATG14:BECN1 sub-complex (Baskaran et al., 2014). Both PIK3C3-C1 and PIK3C3-C2 may associate with other regulatory subunits, including Rubicon autophagy regulator, BIF-1, autophagy and beclin 1 regulator 1, and nuclear receptor binding factor 2 (NRBF2) (Matsunaga et al., 2009; Thoresen et al., 2010; Cao et al., 2014). PIK3C3-C1 is likely related to PIK3CB and interacts with Ras-related protein Rab-7a and NRBF2 (Cao et al., 2014) within the PIK3C3/VPS34 complex (Stein et al., 2003). The PIK3R4 protein mediates the formation of phosphatidylinositol-3-phosphate as the regulatory subunit of the PIK3 complex. Moreover, the different forms of the PI3K complex affect several pathways involving trafficked membranes. PIK3C3-C1 contributes to initiating the autophagosome, maturating both the autophagosome and endocytosis of PIK3C3-C2, and regulating the degradation of endocytic traffic and cytokinesis (Thoresen et al., 2010).

SOD1 transgenic mice are the most commonly used animal model for *in vivo* studies of ALS. PC12 cells possess the morphological characteristics of neural cells and are frequently used in *in vitro* studies of neurological diseases (Kato et al., 2005; McCaffrey, 2006; Zhang et al., 2012; Trippier et al., 2014). Based on previous studies (Rosen et al., 1993; Li et al., 2016; Lu et al., 2016; Liang et al., 2017; Chung et al., 2018; Zhang et al., 2018a, b), we hypothesized that the expression and distribution of abnormal autophagy-related proteins may be part of the pathogenic mechanism of ALS. Many proteins are involved in autophagy, including PIK3R4. The expression of this protein was significantly decreased in the Tg(SOD1*G93A)1Gur (TG) mouse model of ALS in our previous study (Zhang et al., 2018b). Therefore, the aim of this study was to further explore the relationships between PIK3R4 and ALS pathogenesis in these TG mice.

Materials and Methods

Cell line and animals
The PC12 cell line (#RRID: CVCL_F659) was purchased from the Cell Bank of the Chinese Academy of Sciences (Serial: TCR 9) and was originally derived from a rat pheochromocytoma. PC12 cells were cultured at a constant temperature of 37°C and 5% carbon dioxide in low sugar Dulbecco's modified Eagle medium (DMEM; Gibco; Grand Island, NY, USA) containing 10% fetal bovine serum (Gibco). TG mice (Stock No. JAX:004435; Jackson laboratory; Bar Harbor, ME, USA) and wild-type (WT) mice were provided by the Model Animal Research Institute of Nanjing University (license No. SYXK (Su) 2019-0056). All studies and experiments with animals included the rationale for testing animals and were conducted in accordance with the Guide for the Care and Use of Laboratory Animals of China. The mice were housed in a facility maintained at 20–27°C and 40–50% humidity with a 12 hour light/dark cycle and were provided free access to food and water. Protocols were reviewed and approved by the Ethics Committee for Animal Care and Use at Jiangxi Provincial People's Hospital, Affiliated People's Hospital of Nanchang University (approval No. 2020025; approval date: March 26, 2020). All experiments were designed and reported according to the Animal Research: Reporting of *In Vivo* Experiments (ARRIVE) guidelines (Percie du Sert et al., 2020).

Small interfering RNAs for silencing *PIK3R4*
The sequences of small interfering RNAs (siRNAs; Shanghai GenePharma Co. Ltd.; Shanghai, China) were as follows: PIK3R4 siRNA sequences: 5′-GCA CAA AAC UGC UAA AAU TT-3′, 5′-AUU UAC AGC AGA UUU GUG CTT-3′; and negative control siRNA sequences: 5′-UUC UCC GAA CGU GUC ACG UTT-3′, 5′-ACG UGA CAC GUU CGG AGA ATT-3′. The PC12 cells were transfected with PIK3R4 siRNA or negative control siRNA. On the day before transfection, adherent PC12 cells in a logarithmic growth phase were dissociated with trypsin and counted. Then, the appropriate number of cells (approximately $3.0–8.0 × 10^5$ cells/well) were resuspended in fresh culture medium without antibiotics, added to six-well plates, and incubated overnight. For transfection, 250 μL Opti-MEM medium (Gibco) was added to each of two 1.5 mL sterile centrifuge tubes (labeled A and B), and 120 pM siRNA in 250 μL DMEM was added to tube A and gently mixed. Then, 4 μL Lipofectamine® 2000 (Invitrogen; Carlsbad, CA, USA) and 250 μL DMEM were added to tube B and incubated at room temperature for 5 minutes. Next, samples A and B were mixed and incubated at room temperature for 20 minutes. Finally, a total volume of 2 mL of fresh medium containing the transfection reagent mixture was added to the appropriate cells in the six-well plate. After 6 hours, the culture medium was replaced with 90% DMEM/10% fetal bovine serum.

Real-time reverse transcription polymerase chain reaction
For each sample, Trizol (Solarbio, Beijing, China) was added to the PC12 cells and the solution was transferred to an RNAse-free Eppendorf tube. Chloroform was added at a 1:5 ratio of chloroform to Trizol, mixed, and the mixture was centrifuged at $12,000 × g$, 4°C for 20 minutes. The supernatant was transferred to another Eppendorf tube with an equal volume of isopropanol, centrifuged at $12,000 × g$, 4°C for 15 minutes, and the resulting supernatant was discarded. Anhydrous ethanol was added to the RNA precipitate, which was centrifuged at $12,000 × g$, 4°C for 10 minutes, and the supernatant was discarded again. Finally, diethyl pyrocarbonate-treated water was added to dissolve the RNA pellet. The concentration of RNA was measured using a spectrophotometer (Mettler Toledo; Zurich, Switzerland). The extracted RNA was used for reverse transcription polymerase chain reaction (RT-PCR). The experimental steps were as follows: 2 μL 5X PrimeScript™ RT Master Mix (TaKaRa Bio, Tokyo, Japan), 2 μL total RNA, and RNase free ddH$_2$O

were added to a final volume of 10 μL/tube. The reverse transcription reaction was performed at 37°C for 15 minutes, and the reverse transcriptase was inactivated at 85°C for 5 seconds.

The PCR primers were purchased from Beijing Liuhe Huada Gene Technology Co., Ltd. (Beijing, China). The β-actin forward-primer was 5′-CTG AGA GGG GAA AAT CGT GCG TGA C-3′, and the reverse-primer was 5′-AGG AAG GAG GAT GCA GTG G-3′. The PIK3R4 forward-primer was 5′-GAA CTT CAA GCA GCT CAT ACA AC-3′, and the reverse-primer was 5′-GCT CAT GAA GAT GTG CAA CTAG-3′. The preparation of the quantitative PCR solution was performed on ice and each reaction consisted of 10 μL TB Green Premix Ex Taq II reagent (Takara), 0.8 μL of each gene-specific forward and reverse PCR primers, 0.4 μL ROX Reference Dye II (Takara), 2 μL complementary DNA solution (Takara), and 6 μL distilled H$_2$O. The standard PCR amplification procedure was as follows: one cycle of denaturation at 95°C for 30 seconds followed by 40 cycles comprising 95°C for 5 seconds and 60°C for 30 seconds. After amplification, we observed the amplification and melt curves for the quantitative PCR and obtained the effective cycle threshold (Ct) values, which were analyzed using GraphPad Prism 7 software (GraphPad Software, Inc., La Jolla, CA, USA).

Cell proliferation assay
Cell proliferation was measured using the Cell Counting Kit-8 (CCK-8; Dojindo; Kumamoto, Japan). After a 24-hour transfection, 100 μL cells/well were added to a 96-well plate and 10 μL CCK-8 solution was added to each well. The transfected cells were incubated in CCK-8 solution for 1–4 hours at 37°C. Absorbance at 450 nm was detected using a microplate reader (Thermo Fisher; Waltham, MA, USA).

Genotyping of TG mice
Interleukin-2 (IL-2) primers were used as a positive internal control. DNA from the tails of the TG mice was examined by PCR. As in our previous study (Zhou et al., 2015; Zhang et al., 2018b; Zhang et al., 2018a), the 5′-CTA GGC CAC AGA ATT GAA AGA TCT-3′ sequence was used as the IL-2 forward-primer and 5′-GTA GGT GGA AAT TCT AGC ATC ATC C-3′ as the IL-2 reverse-primer. For detection of the human SOD1G93A mutation, the sequence 5′-CAT CAG CCC TAA TCC ATC TGA-3′ was used as the forward-primer and 5′-CGC GAC TAA CAA TCA AAG TGA-3′ as the reverse-primer. The primers were synthesized by Beijing Liuhe Huada Gene Company (Beijing, China). The amplification conditions were set at 94°C denaturation for 3 seconds, 60°C annealing for 1 minute, and 72°C extension for 1 minute; the number of cycles was 35.

Experimental groups of mice and sample preparation
Eighteen TG and 18 WT mice were randomly selected for the experimental and control groups, respectively. Each stage (60–70 days; 90–100 days; 120–130 days) consisted of six TG and six WT mice. After the genotypic identification of the mice, TG and WT mice were randomly selected for a blinded immunohistochemical staining analysis. After staining, we matched the results of each sample to its true identity and summarized these data.

TG mice were sacrificed at 60–70 days (pre-onset stage), 90–100 days (onset stage), or 120–130 days (progression stage), and WT mice were sacrificed on the same days as controls. At each stage of disease, the gastrocnemius muscles were removed, sectioned, and examined using hematoxylin-eosin staining, and changes in muscle structure were observed by light microscopy (Nikon; Tokyo, Japan) to evaluate the different disease stages (Rosen et al., 1993; Henriques et al., 2010; Zhou et al., 2015). The hematoxylin-eosin staining procedure was as follows: the sections were washed for 1 minute, incubated with Mayer's hematoxylin solution for

5 minutes, washed again for 10 minutes, and immersed for 3 minutes in a solution containing 1% acetic acid with 0.5% eosin. After washing three times, the sections were dehydrated successively in 70% ethyl alcohol for 1 minute, 90% ethyl alcohol for 30 seconds, 100% ethyl alcohol for 30 seconds, and xylene for 30 seconds. These protocols were previously described (Zhou et al., 2015). No animals or data points were excluded from the analysis.

Fluorescent immunohistochemical staining
For fluorescent immunohistochemical staining, WT and TG mice were anesthetized using a solution of 10% chloral hydrate (Merck, Darmstadt, Germany) with 3% sodium pentobarbital (Merck) and then perfused at room temperature with 20 mL normal saline followed by 40 mL 4% paraformaldehyde in 1× phosphate buffer saline (PBS, pH 7.5). The spinal cords were excised and placed in 4% paraformaldehyde overnight, incubated in 20% sucrose in 1× PBS, pH 7.5, and embedded in OCT freezing medium (Sakura Finetek USA, Inc., Torrance, CA, USA). Spinal cords were cut from the rostral to caudal side into 12-μm-thick sections using a cryostat (Leica; Wetzlar, Germany), and the sections were placed on Superfrost Plus slides (Citotest; Haimen, China). Sections were rehydrated in 1× PBS (pH 7.4), permeabilized with 0.2% Triton X-100, and blocked with 10% bovine albumin dissolved in 1× PBS. The sections were incubated with anti-PIK3R4 (1:100; RRID: AB_11141464; rabbit; Cat# ab128903; Abcam; Cambridge, MA, USA) and anti-NeuN (1:200; RRID: AB_10711040; mouse; Cat# ab104224, Abcam) antibodies at 4°C overnight and washed 6× in 0.2% Triton X-100/1× PBS for 5–10 minutes per wash. The sections were incubated with cyanine-3-conjugated goat anti-rabbit IgG (1:200; RRID: AB_2890957; Cat# SA00009-2; Proteintech China; Wuhan, Hubei, China) and fluorescein isothiocyanate-conjugated donkey anti-mouse IgG (1:200; RRID: AB_2857366; Cat# SA00003-9; Proteintech China) for 2 hours at room temperature. After adequately washing, the sections were covered with antifade medium and observed with a Nikon E800 fluorescent microscope. Images were captured with a spot digital camera (Diagnostic Instruments; Sterling Heights, MI, USA) and analyzed using Photoshop CC 2019 software (Adobe Systems; San Jose, CA, USA).

Western blot assay
Protein extraction and quantification procedures were conducted for PC12 cells after PIK3R4 silencing with siRNA as follows. Lysis buffer (100–150 μL) containing 1 mM phenylmethylsulfonyl fluoride was added to PC12 cells in each well of the six-well plates. The cell lysate solutions were centrifuged at 14,000 × g for 3–5 minutes at 4°C, and the supernatants were collected. Protein concentrations were quantified using a bicinchoninic acid kit (Solarbio). The operation steps for spinal protein extraction and quantification were as follows. Mice in each group were sacrificed after the animals were anesthetized with a solution of 10% chloral hydrate as a sedative combined with 20% urethane analgesia. The mice were quickly placed on ice, and the spinal cords were carefully separated. From each mouse, 30 mg of lumbar spinal cord was removed and transferred to a 1.5 mL Eppendorf tube, and 200 μL pre-cooled lysis buffer was added. An electronic tissue grinder was used to grind the lumbar cord until there were no obvious particles. After 2 hours of lysis, the tissue lysate was centrifuged at 12,000 × g for 10 minutes at 4°C, and the supernatant was collected.

Western blots were used for the semi-quantitative analysis of spinal proteins in each mouse group. Proteins (20–40 μg) were separated by sodium dodecyl sulfate-polyacrylamide gel electrophoresis and transferred to the polyvinylidene fluoride membranes (Millipore; Bedford, MA, USA). Membranes were blocked with 5% skim milk in PBS for 1 hour at room temperature and incubated with primary antibodies. The concentrations of primary antibodies were as follows: anti-

glyceraldehyde-3-phosphate dehydrogenase (1:2000; RRID: AB_2263076; rabbit; Cat# 10494-1-AP; Proteintech China); anti-PIK3R4 (1:2000; RRID: AB_11141464; rabbit; Cat# ab128903; Abcam), anti-SOD1 (1:2000; RRID: AB_2193750; rabbit; Cat# 10269-1-AP; Proteintech China), anti-sequestosome 1 (SQSTM1, p62; 1:1000; RRID: AB_2810880; rabbit; Cat# ab109012; Abcam) and anti-microtubule-associated proteins 1A/1B light chain 3 (LC3; 1:2000; RRID: AB_2137737; rabbit; Cat# 14600-1-AP; Proteintech China). Horseradish peroxidase-conjugated goat anti-rabbit IgG (1:1500–2500; RRID: AB_2722564; Cat# SA00001-2; Proteintech China) was selected as the secondary antibody. Chemiluminescence was evaluated using the BeyoECL Plus Kit (Beyotime; Shanghai, China), and the detailed procedures were previously described (Zhang et al., 2018b). Image J software (National Institute of Health; Bethesda, MD, USA) was used to analyze protein band densities. Relative protein expression was normalized to glyceraldehyde-3-phosphate dehydrogenase, a house-keeping protein.

Statistical analysis
Statistical methods were not used to predetermine sample sizes; however, our sample sizes are similar to those reported in a previous publication (Zhou et al., 2015). Data were analyzed and plotted using GraphPad Prism 7. Experimental data are presented as mean ± standard deviation (SD). Comparisons of three or more groups were conducted using one-way analysis of variance followed by Tukey's *post hoc* tests, and the Student's *t*-test was employed for comparisons between two groups. $P < 0.05$ was considered statistically significant.

Results
Efficiency of PIK3R4 silencing by siRNA in PC12 cells
At 24 hours after siRNA transfection, quantitative PCR showed the mRNA expression of PIK3R4 in the siRNA-PIK3R4 group was decreased compared with the negative control ($P = 0.0011$) and non-transfected groups ($P = 0.0004$; **Figure 1A**).

Transfection with PIK3R4 siRNA does not affect cell proliferation in PC12 cells
Cell proliferation in the siRNA-PIK3R4, negative control, and non-transfected groups was not significantly different at 24, 48, and 72 hours after transfection. The results were analyzed using one-way analysis of variance followed by Tukey's *post hoc* tests ($P > 0.05$; **Figure 1B**).
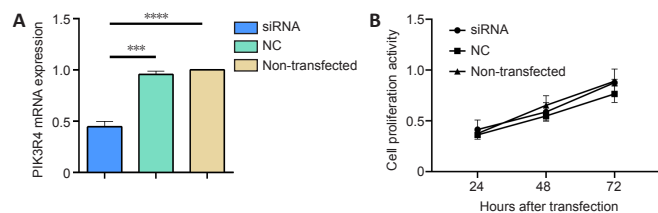
Figure 1 | Effect of PIK3R4-siRNA interference on PIK3R4 mRNA expression and cell proliferation of PC12 cells.
(A) PIK3R4 mRNA expression ($2^{-\Delta\Delta CT}$) detected by real-time, fluorescent, quantitative reverse transcription polymerase chain reaction. (B) Cell proliferation activity (optical density at 490 nm) detected using the Cell Counting Kit-8. Data are presented as the mean ± SD. The experiment was repeated three times. ***$P < 0.001$, ****$P < 0.0001$ (Student's *t*-test). NC: Negative control group; PIK3R4: phosphoinositide-3-kinase regulatory subunit 4; siRNA: siRNA-PIK3R4 group.

Transfection with PIK3R4 siRNA decreases the protein expression of PIK3R4, p62, and LC3 in PC12 cells
Western blot results demonstrated that transfection of PC12 cells with PIK3R4 siRNA markedly decreased the protein expression of PIK3R4, p62, and LC3 compared with the non-transfected group (**Figure 2A**). Differences in the relative

protein levels between the two groups are shown in **Figure 2B–D** (PIK3R4: $P = 0.0353$, p62: $P = 0.0088$, LC3: $P = 0.0106$). SOD1 expression was slightly decreased in the PIK3R4 siRNA group compared with the non-transfected group ($P = 0.0487$; **Figure 2A** and **E**).
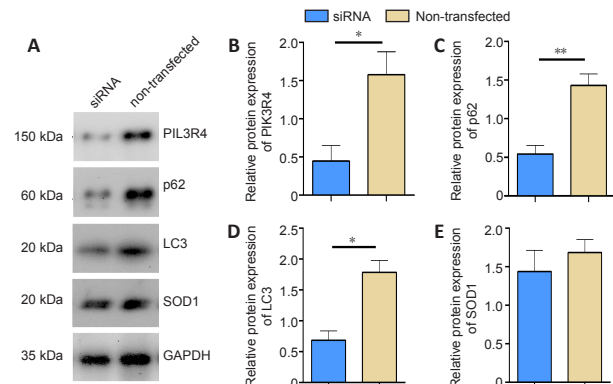
Figure 2 | Effect of PIK3R4-siRNA interference on the protein expression of PIK3R4, p62, LC3, and SOD1 in PC12 cells.
(A) Protein bands of PIK3R4, p62, LC3, and SOD1 detected by western blot assays. (B–E) Quantitative results for PIK3R4 (B), p62 (C), LC3 (D), and SOD1 (E) protein expression. Relative protein expression was normalized to GAPDH. Data are expressed as the mean ± SD. The experiment was repeated three times. *$P < 0.05$, **$P < 0.01$ (Student's *t*-test). GAPDH: Glyceraldehyde-3-phosphate dehydrogenase; LC3: microtubule associated protein 1 light chain 3; SOD1: superoxide dismutase 1; PIK3R4: phosphoinositide-3-kinase regulatory subunit 4; siRNA: siRNA-PIK3R4 group.

PIK3R4 protein is distributed in cervical, thoracic, and lumbar segments of the spinal cord in TG mice
Immunofluorescence staining demonstrated that PIK3R4-positive cells were extensively distributed in the anterior horn, central canal, the area surrounding the central canal, and the posterior horn of the cervical, thoracic, and lumbar segments of the spinal cord during the pre-onset, onset, and progression stages in both the WT and TG mice (**Figure 3**). PIK3R4-positive cells decreased in the anterior horn of the cervical, thoracic, and lumbar cord segments of TG mice during progression (**Figure 3**). Based on "rough" observations using fluorescence microscopy, the general tendency was decreased PIK3R4 distribution in the spinal cord of TG mice at pre-onset, onset, and progression stages compared with WT mice. However, a detailed fluorescence data analysis was not performed.

PIK3R4 is expressed and distributed in neurons of spinal lumbar segments in TG mice
Immunofluorescence staining showed that PIK3R4 was extensively expressed and distributed within NeuN-positive neuronal cells in the anterior horn, posterior horn, and central canal of the spinal lumbar segments. PIK3R4 expression and distribution in neurons of the spinal lumbar segments were not significantly changed between WT and TG mice at the pre-onset, onset, and progression timepoints (**Figure 4**).

Protein expression of PIK3R4, p62, LC3, and SOD1 is altered in the spinal lumbar segments of TG mice
PIK3R4 protein expression in TG mice was significantly decreased at both pre-onset and onset stages, and significantly increased at the progression stage in comparison with the equivalent timepoints for WT mice (pre-onset: $P = 0.0036$, onset: $P = 0.0459$, progression: $P = 0.0487$; **Figure 5A** and **B**). The expression of p62 was significantly decreased at the pre-onset stage ($P = 0.0081$) and significantly increased at the progression stage in the TG group ($P = 0.011$) compared with the corresponding WT groups (**Figure 5A, C**). LC3 protein expression was not significantly different between the WT and TG mice at the different stages (pre-onset: $P = 0.9678$, onset: $P = 0.7698$, progression: $P = 0.8141$; **Figure 5A, D**), and SOD1 was only expressed in the TG mice (**Figure 5A**).
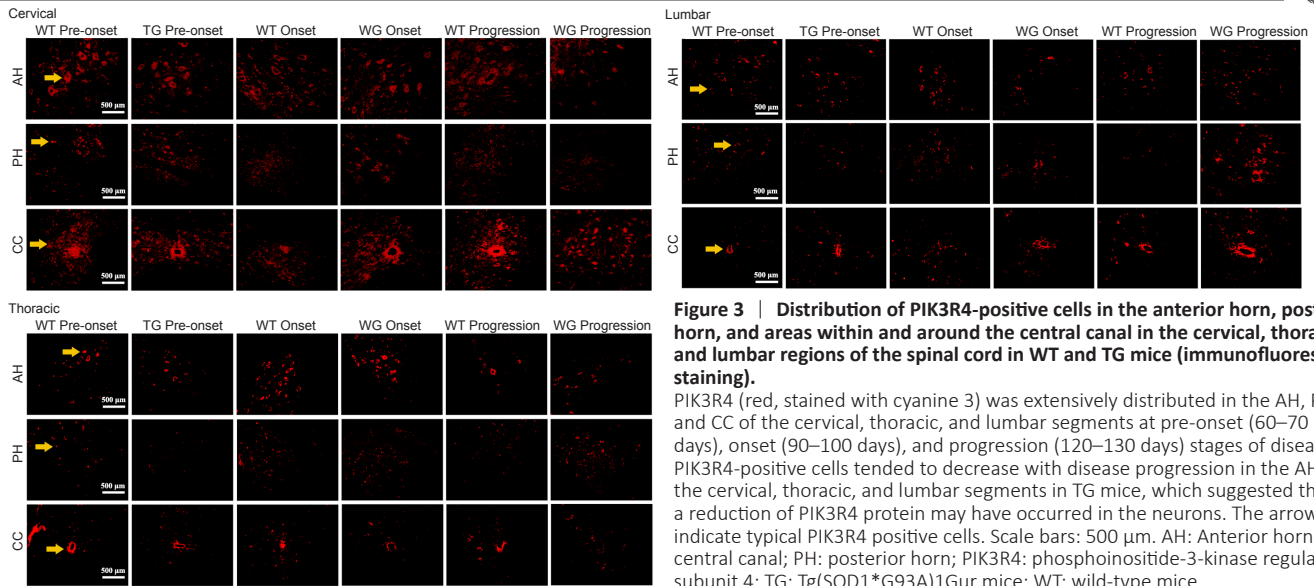
Figure 3 | Distribution of PIK3R4-positive cells in the anterior horn, posterior horn, and areas within and around the central canal in the cervical, thoracic, and lumbar regions of the spinal cord in WT and TG mice (immunofluorescence staining).

PIK3R4 (red, stained with cyanine 3) was extensively distributed in the AH, PH, and CC of the cervical, thoracic, and lumbar segments at pre-onset (60–70 days), onset (90–100 days), and progression (120–130 days) stages of disease. PIK3R4-positive cells tended to decrease with disease progression in the AH of the cervical, thoracic, and lumbar segments in TG mice, which suggested that a reduction of PIK3R4 protein may have occurred in the neurons. The arrows indicate typical PIK3R4 positive cells. Scale bars: 500 μm. AH: Anterior horn; CC: central canal; PH: posterior horn; PIK3R4: phosphoinositide-3-kinase regulatory subunit 4; TG: Tg(SOD1*G93A)1Gur mice; WT: wild-type mice.
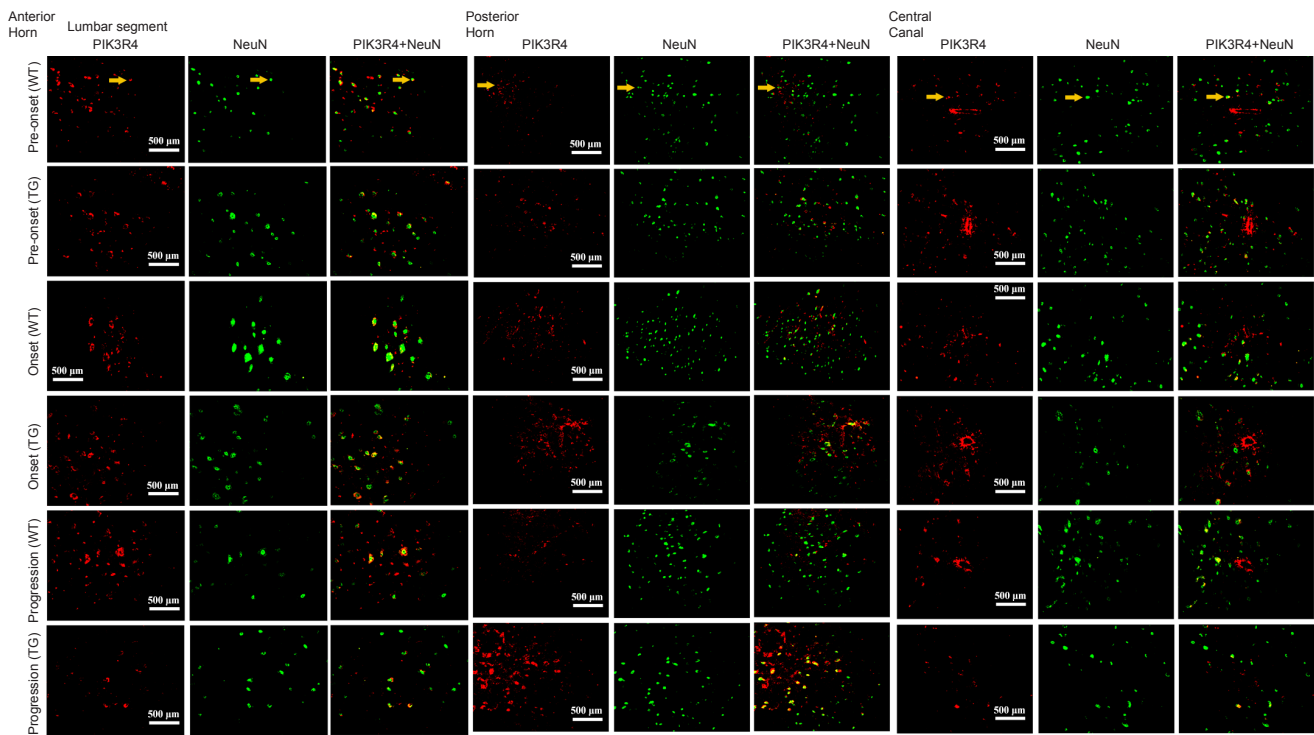

Figure 4 | PIK3R4 and NeuN double-positive cells in the AH, PH, and areas around the CC of the spinal lumbar segment at different stages in both WT and TG mice (immunofluorescence staining).

PIK3R4-positive cells (red, stained with cyanine 3) overlapped extensively with NeuN-positive cells (green, stained with fluorescein isothiocyanate) in the AH, PH, and CC at pre-onset (60–70 days), onset (90–100 days), and progression (120–130 days) stages in both WT and TG mice, which indicated that PIK3R4 expression was present in neurons. Scale bars: 500 μm. AH: Anterior horn; CC: central canal; PH: posterior horn; PIK3R4: phosphoinositide-3-kinase regulatory subunit 4; TG: transgenic mice; WT: wild-type mice.
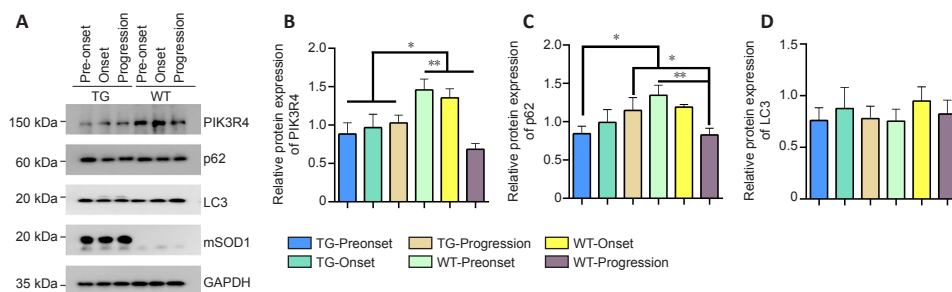

Figure 5 | Protein expression of PIK3R4, p62, LC3, and SOD1 in the spinal lumbar segments of WT and TG mice at different stages.

(A) Protein bands of PIK3R4, p62, and LC3 detected by western blot assay. (B) Quantitative results of PIK3R4 (B), p62 (C), and LC3 (D) protein expression. Relative protein expression was normalized to GAPDH. Data are presented as the mean ± SD. Three technical replicates were performed for each mouse (3 mice per group). *$P < 0.05$, **$P < 0.01$ (Student's t-test). GAPDH: Glyceraldehyde-3-phosphate dehydrogenase; LC3: microtubule associated protein 1 light chain 3; mSOD1: mutant superoxide dismutase 1; PIK3R4: phosphoinositide-3-kinase regulatory subunit 4; siRNA: siRNA-PIK3R4 group.

Discussion

In this study, we described changes in the expression and distribution of PIK3R4 and its related proteins in cell and animal experiments. Although cell survival was not significantly changed in the *in vitro* experiments, the autophagy-related proteins p62 and LC3 were significantly downregulated, and the SOD1 protein was slightly downregulated when PIK3R4 expression was reduced by siRNA. In the ALS animal model (TG mice), the PIK3R4 protein was abundantly expressed and distributed in the anterior horn, central canal, area surrounding the central canal, and posterior horn of the spine. Furthermore, PIK3R4 protein expression was found within the neurons of these spinal regions. In TG mice, the expression of PIK3R4 and p62 showed a decreasing trend in the pre-onset and onset stages and an increasing trend during the progression stage of the disease. LC3 protein expression did not change significantly in the spinal cord. We also propose that there was a tendency for a decrease in PIK3R4 positive cells in the anterior horn of each spinal cord segment of TG mice at the progression stage.

PIK3R4 is an important component of the autophagy process (Ohashi et al., 2016). Mutations in PIK3R4 can lead to a defect in neuronal migration and, eventually, to a rupture in the hippocampal pyramidal cell layer. Complete ablation of PIK3R4 can lead to the accumulation of autophagy substrates, which may induce apoptosis and severe cortical atrophy (Gstrein et al., 2018). In addition, mice lacking PIK3R4 in skeletal muscle may suffer from severe myopathy (Nemazanyy et al., 2013). Therefore, PIK3R4 protein is closely related to the development of lesions in skeletal muscle. As an important autophagy-related protein, p62 is a receptor protein that specifically binds to autophagy substrates. In this study, p62 protein was decreased at the pre-onset stage of disease in TG mice, suggesting a decrease in autophagy substrate binding. In PC12 cells, the down-regulation of PIK3R4 protein by siRNA transfection resulted in decreased expression of the autophagy biomarkers p62 and LC3 proteins. Despite the downregulation of PIK3R4, p62, and LC3 proteins, PC12 cell proliferation was not altered. The decreased expression of p62 and LC3 proteins suggested autophagy was decreased. Therefore, the downregulation of PIK3R4 protein may lead to a decrease in autophagy and maintenance of survival of PC12 cells. In the mouse study, PIK3R4 and p62 proteins were significantly downregulated at the pre-onset and onset stages and upregulated at the progression stage of ALS in TG mice compared with WT mice at the corresponding timepoints. Downregulation of PIK3R4 and p62 protein at the early stages may allow the self-repair of neuronal cells by preventing autophagy and upregulation at the later stage may promote autophagy-mediated neuronal degeneration. PIK3R4 may be a part of the ALS pathogenic mechanism by regulating autophagy. Therefore, preventing abnormal PIK3R4 downregulation in the early stages of the disease may be a potential target for ALS treatment and a method for preventing the progression of ALS.

In the ALS neurodegenerative process, related cellular mechanisms have been discovered, such as RNA imbalance, abnormal protein homeostasis, and mitochondrial dysfunction. Aggregates of insoluble proteins, mitochondrial lesions, and stress particles containing RNAs and proteins are recognized and promptly degraded via selective autophagy. The relationship between autophagy disorders and neurodegenerative diseases, including ALS, has been confirmed by several studies (Hara et al., 2006; Guo et al., 2018; Vicencio et al., 2020). Autophagy in neurons exerts a protective effect under steady state conditions. In mice lacking autophagy essential genes in the central nervous system, such as Atg5 and Atg7, the extensive accumulation of ubiquitinated cytoplasmic inclusion bodies is a feature of neurodegeneration (Hara et al., 2006; Komatsu et al., 2006). The most obvious evidence that autophagy participates in the ALS pathophysiological process is the accumulation of autophagy-related features in the spinal neurons of ALS patients (Sasaki, 2011).

The majority of studies on the pathophysiological mechanisms of ALS have been performed using ALS models. Mutant SOD1 mouse models have been extensively applied to study ALS pathogenesis (Nassif et al., 2014; Rudnick et al., 2017; Mitsui et al., 2018; Beltran et al., 2019; Li et al., 2019). The mutant SOD1 mouse model showed that, through the visualization of yeast Atg8 homologs (mainly LC3-II), autophagy increased, and mTOR activity decreased (Saxena et al., 2013). In Tg(SOD1*G93A)1Gur mice, an increase in p62 levels coincided with an increase in autophagy (Gal et al., 2007; An et al., 2014). The p62 (SQSTM1) protein was the first autophagy receptor to be discovered and was shown to bind to ubiquitinated substrates to mediate transfer to the autophagosome for subsequent degradation, thereby maintaining protein homeostasis (Tung et al., 2010). The levels of p62 are often considered an indicator of autophagy activity because p62 is degraded together with its substrate. It is worth noting that p62 is expressed in motor neurons of the spinal cord, and p62 gene mutations account for approximately 1% of ALS cases (Rudnick et al., 2017). Mutations of p62 located in the LC3-interacting region domain indicate the influence of selective autophagy on the pathogenesis of ALS (Fecto et al., 2011). Acting as a scaffold protein, p62 also plays a key regulatory role in a variety of signal transduction pathways, such as amino acid sensing, oxidative stress, DNA damage response, nuclear factor kappa beta activation, cell death, and ubiquitin-mediated degradation through the proteasome and autophagy (Deosaran et al., 2013; Zhang et al., 2014; Goodall et al., 2016; Salazar et al., 2020).

This study had the following deficiencies. First, because only a cell line was transfected with siRNA to downregulate the PIK3R4 protein, the degree of evidence for the functional mechanism of PIK3R4 in ALS is poor. Further studies that upregulate this protein in an *in vitro* ALS model may be useful to observe cell survival activity and misfolded protein aggregation. Second, the number of animals per group was small in our study, and the PIK3R4 immunofluorescent staining was not sufficient to quantitate the differences in PIK3R4 expression and distribution. We observed the expression and distribution in different anatomical regions of the spinal cord for both WT and TG mice at the pre-onset, onset, and progression stages. However, expression differences may exist between the WT and TG mice in other anatomical sites and at different timepoints during disease progression, and the exact alterations require further investigation. Furthermore, although we observed the distribution and expression of PIK3R4 *in vivo*, molecular interventions were not performed in the ALS mice, which has led to a limited understanding of the possible phenotypic changes brought by regulation of PIK3R4 in ALS.

In summary, the autophagy-related proteins p62 and LC3 were significantly downregulated after downregulation of PIK3R4 protein in PC12 cells, which implied that PIK3R4 may prevent autophagy by regulating the expression of p62 and LC3. The PIK3R4 protein was abundantly expressed and distributed in the neurons of the spinal anterior horn, central canal and surrounding area, and posterior horn. In the animal model of ALS, the expression of PIK3R4 and p62 decreased in the pre-onset and onset stages and increased in the progression stage of disease. These data demonstrated that PIK3R4 and p62 decreased in ALS as a whole. Second, because levels of these proteins were increased during disease progression, our data

suggest that autophagy played a role in self-protection but could not reverse disease progression. Finally, the autophagy pathway may be a method to prevent the progression of ALS disease by promoting autophagy to reduce the accumulation of abnormal proteins, thus prolonging the survival of ALS mice. However, this hypothesis requires further study. In conclusion, our data suggest that PIK3R4 may prevent the progression of ALS by regulating autophagy.

References

An T, Shi P, Duan W, Zhang S, Yuan P, Li Z, Wu D, Xu Z, Li C, Guo Y (2014) Oxidative stress and autophagic alteration in brainstem of SOD1-G93A mouse model of ALS. Mol Neurobiol 49:1435-1448.

Baskaran S, Carlson LA, Stjepanovic G, Young LN, Kim DJ, Grob P, Stanley RE, Nogales E, Hurley JH (2014) Architecture and dynamics of the autophagic phosphatidylinositol 3-kinase complex. Elife 3:e05115.

Beltran S, Nassif M, Vicencio E, Arcos J, Labrador L, Cortes BI, Cortez C, Bergmann CA, Espinoza S, Hernandez MF, Matamala JM, Bargsted L, Matus S, Rojas-Rivera D, Bertrand MJM, Medinas DB, Hetz C, Manque PA, Woehlbier U (2019) Network approach identifies Pacer as an autophagy protein involved in ALS pathogenesis. Mol Neurodegener 14:14.

Boillée S, Vande Velde C, Cleveland DW (2006) ALS: a disease of motor neurons and their nonneuronal neighbors. Neuron 52:39-59.

Cai B, Fan DS (2013) Germline degradation of a mouse model of familial amyotrophic lateral sclerosis when breeding. Zhongguo Zuzhi Gongcheng Yanjiu 17:4521-4528.

Cao Y, Wang Y, Abi Saab WF, Yang F, Pessin JE, Backer JM (2014) NRBF2 regulates macroautophagy as a component of Vps34 complex I. Biochem J 461:315-322.

Chen L (2021) The important functional role of TDP-43 plays in amyotrophic lateral sclerosis-frontotemporal dementia. Neural Regen Res 16:682-683.

Cheon SY, Kim H, Rubinsztein DC, Lee JE (2019) Autophagy, cellular aging and age-related human diseases. Exp Neurobiol 28:643-657.

Chung CG, Lee H, Lee SB (2018) Mechanisms of protein toxicity in neurodegenerative diseases. Cell Mol Life Sci 75:3159-3180.

Codogno P, Ogier-Denis E, Houri JJ (1997) Signal transduction pathways in macroautophagy. Cell Signal 9:125-130.

Deosaran E, Larsen KB, Hua R, Sargent G, Wang Y, Kim S, Lamark T, Jauregui M, Law K, Lippincott-Schwartz J, Brech A, Johansen T, Kim PK (2013) NBR1 acts as an autophagy receptor for peroxisomes. J Cell Sci 126:939-952.

Fecto F, Yan J, Vemula SP, Liu E, Yang Y, Chen W, Zheng JG, Shi Y, Siddique N, Arrat H, Donkervoort S, Ajroud-Driss S, Sufit RL, Heller SL, Deng HX, Siddique T (2011) SQSTM1 mutations in familial and sporadic amyotrophic lateral sclerosis. Arch Neurol 68:1440-1446.

Fogel AI, Dlouhy BJ, Wang C, Ryu SW, Neutzner A, Hasson SA, Sideris DP, Abeliovich H, Youle RJ (2013) Role of membrane association and Atg14-dependent phosphorylation in beclin-1-mediated autophagy. Mol Cell Biol 33:3675-3688.

Gal J, Ström AL, Kilty R, Zhang F, Zhu H (2007) p62 accumulates and enhances aggregate formation in model systems of familial amyotrophic lateral sclerosis. J Biol Chem 282:11068-11077.

Goodall ML, Fitzwalter BE, Zahedi S, Wu M, Rodriguez D, Mulcahy-Levy JM, Green DR, Morgan M, Cramer SD, Thorburn A (2016) The autophagy machinery controls cell death switching between apoptosis and necroptosis. Dev Cell 37:337-349.

Gstrein T, Edwards A, Přistoupilová A, Leca I, Breuss M, Pilat-Carotta S, Hansen AH, Tripathy R, Traunbauer AK, Hochstoeger T, Rosoklija G, Repic M, Landler L, Stránecký V, Dürnberger G, Keane TM, Zuber J, Adams DJ, Flint J, Honzik T, et al. (2018) Publisher Correction: Mutations in Vps15 perturb neuronal migration in mice and are associated with neurodevelopmental disease in humans. Nat Neurosci 21:1139.

Guo F, Liu X, Cai H, Le W (2018) Autophagy in neurodegenerative diseases: pathogenesis and therapy. Brain Pathol 28:3-13.

Hara T, Nakamura K, Matsui M, Yamamoto A, Nakahara Y, Suzuki-Migishima R, Yokoyama M, Mishima K, Saito I, Okano H, Mizushima N (2006) Suppression of basal autophagy in neural cells causes neurodegenerative disease in mice. Nature 441:885-889.

Henriques A, Pitzer C, Schneider A (2010) Characterization of a novel SOD-1(G93A) transgenic mouse line with very decelerated disease development. PLoS One 5:e15445.

Jung S, Jeong H, Yu SW (2020) Autophagy as a decisive process for cell death. Exp Mol Med 52:921-930.

Kato S, Kato M, Abe Y, Matsumura T, Nishino T, Aoki M, Itoyama Y, Asayama K, Awaya A, Hirano A, Ohama E (2005) Redox system expression in the motor neurons in amyotrophic lateral sclerosis (ALS): immunohistochemical studies on sporadic ALS, superoxide dismutase 1 (SOD1)-mutated familial ALS, and SOD1-mutated ALS animal models. Acta Neuropathol 110:101-112.

Komatsu M, Waguri S, Chiba T, Murata S, Iwata J, Tanida I, Ueno T, Koike M, Uchiyama Y, Kominami E, Tanaka K (2006) Loss of autophagy in the central nervous system causes neurodegeneration in mice. Nature 441:880-884.

Li J, Song M, Moh S, Kim H, Kim DH (2019) Cytoplasmic restriction of mutated SOD1 impairs the DNA repair process in spinal cord neurons. Cells 8:1502.

Li J, Lu Y, Liang H, Tang C, Zhu L, Zhang J, Xu R (2016) Changes in the expression of FUS/TLS in spinal cords of SOD1 G93A transgenic mice and correlation with motor-neuron degeneration. Int J Biol Sci 12:1181-1190.

Liang H, Wu C, Deng Y, Zhu L, Zhang J, Gan W, Tang C, Xu R (2017) Aldehyde dehydrogenases 1A2 expression and distribution are potentially associated with neuron death in spinal cord of Tg(SOD1*G93A)1Gur mice. Int J Biol Sci 13:574-587.

Lu Y, Tang C, Zhu L, Li J, Liang H, Zhang J, Xu R (2016) The overexpression of TDP-43 protein in the neuron and oligodendrocyte cells causes the progressive motor neuron degeneration in the SOD1 G93A transgenic mouse model of amyotrophic lateral sclerosis. Int J Biol Sci 12:1140-1149.

Ludolph AC, Brettschneider J, Weishaupt JH (2012) Amyotrophic lateral sclerosis. Curr Opin Neurol 25:530-535.

Matsunaga K, Saitoh T, Tabata K, Omori H, Satoh T, Kurotori N, Maejima I, Shirahama-Noda K, Ichimura T, Isobe T, Akira S, Noda T, Yoshimori T (2009) Two Beclin 1-binding proteins, Atg14L and Rubicon, reciprocally regulate autophagy at different stages. Nat Cell Biol 11:385-396.

McCaffrey P (2006) SOD1 mutant protein gets loose in ALS. Lancet Neurol 5:119.

Mitchell JD, Borasio GD (2007) Amyotrophic lateral sclerosis. Lancet 369:2031-2041.

Mitsui S, Otomo A, Nozaki M, Ono S, Sato K, Shirakawa R, Adachi H, Aoki M, Sobue G, Shang HF, Hadano S (2018) Systemic overexpression of SQSTM1/p62 accelerates disease onset in a SOD1(H46R)-expressing ALS mouse model. Mol Brain 11:30.

Nassif M, Valenzuela V, Rojas-Rivera D, Vidal R, Matus S, Castillo K, Fuentealba Y, Kroemer G, Levine B, Hetz C (2014) Pathogenic role of BECN1/Beclin 1 in the development of amyotrophic lateral sclerosis. Autophagy 10:1256-1271.

Nemazanyy I, Blaauw B, Paolini C, Caillaud C, Protasi F, Mueller A, Proikas-Cezanne T, Russell RC, Guan KL, Nishino I, Sandri M, Pende M, Panasyuk G (2013) Defects of Vps15 in skeletal muscles lead to autophagic vacuolar myopathy and lysosomal disease. EMBO Mol Med 5:870-890.

Ohashi Y, Soler N, García Ortegón M, Zhang L, Kirsten ML, Perisic O, Masson GR, Burke JE, Jakobi AJ, Apostolakis AA, Johnson CM, Ohashi M, Ktistakis NT, Sachse C, Williams RL (2016) Characterization of Atg38 and NRBF2, a fifth subunit of the autophagic Vps34/PIK3C3 complex. Autophagy 12:2129-2144.

Panaretou C, Domin J, Cockcroft S, Waterfield MD (1997) Characterization of p150, an adaptor protein for the human phosphatidylinositol (PtdIns) 3-kinase. Substrate presentation by phosphatidylinositol transfer protein to the p150.Ptdins 3-kinase complex. J Biol Chem 272:2477-2485.

Percie du Sert N, Hurst V, Ahluwalia A, Alam S, Avey MT, Baker M, Browne WJ, Clark A, Cuthill IC, Dirnagl U, Emerson M, Garner P, Holgate ST, Howells DW, Karp NA, Lazic SE, Lidster K, MacCallum CJ, Macleod M, Pearl EJ, et al. (2020) The ARRIVE guidelines 2.0: Updated guidelines for reporting animal research. PLoS Biol 18:e3000410.

Rosen DR, Siddique T, Patterson D, Figlewicz DA, Sapp P, Hentati A, Donaldson D, Goto J, O'Regan JP, Deng HX, et al. (1993) Mutations in Cu/Zn superoxide dismutase gene are associated with familial amyotrophic lateral sclerosis. Nature 362:59-62.

Rudnick ND, Griffey CJ, Guarnieri P, Gerbino V, Wang X, Piersaint JA, Tapia JC, Rich MM, Maniatis T (2017) Distinct roles for motor neuron autophagy early and late in the SOD1(G93A) mouse model of ALS. Proc Natl Acad Sci U S A 114:E8294-e8303.

Salameh JS, Brown RH, Jr., Berry JD (2015) Amyotrophic lateral sclerosis: review. Semin Neurol 35:469-476.

Salazar G, Cullen A, Huang J, Zhao Y, Serino A, Hilenski L, Patrushev N, Forouzandeh F, Hwang HS (2020) SQSTM1/p62 and PPARGC1A/PGC-1alpha at the interface of autophagy and vascular senescence. Autophagy 16:1092-1110.

Sasaki S (2011) Autophagy in spinal cord motor neurons in sporadic amyotrophic lateral sclerosis. J Neuropathol Exp Neurol 70:349-359.

Saxena S, Roselli F, Singh K, Leptien K, Julien JP, Gros-Louis F, Caroni P (2013) Neuroprotection through excitability and mTOR required in ALS motoneurons to delay disease and extend survival. Neuron 80:80-96.

Stein MP, Feng Y, Cooper KL, Welford AM, Wandinger-Ness A (2003) Human VPS34 and p150 are Rab7 interacting partners. Traffic 4:754-771.

Thoresen SB, Pedersen NM, Liestøl K, Stenmark H (2010) A phosphatidylinositol 3-kinase class III sub-complex containing VPS15, VPS34, Beclin 1, UVRAG and BIF-1 regulates cytokinesis and degradative endocytic traffic. Exp Cell Res 316:3368-3378.

Trippier PC, Zhao KT, Fox SG, Schiefer IT, Benmohamed R, Moran J, Kirsch DR, Morimoto RI, Silverman RB (2014) Proteasome activation is a mechanism for pyrazolone small molecules displaying therapeutic potential in amyotrophic lateral sclerosis. ACS Chem Neurosci 5:823-829.

Tsai MJ, Hsu CY, Sheu CC (2017) Amyotrophic lateral sclerosis. N Engl J Med 377:1602.

Tung YT, Hsu WM, Lee H, Huang WP, Liao YF (2010) The evolutionarily conserved interaction between LC3 and p62 selectively mediates autophagy-dependent degradation of mutant huntingtin. Cell Mol Neurobiol 30:795-806.

Vicencio E, Beltrán S, Labrador L, Manque P, Nassif M, Woehlbier U (2020) Implications of selective autophagy dysfunction for ALS pathology. Cells 9:381.

Xu RS, Yuan M (2021) Considerations on the concept, definition, and diagnosis of amyotrophic lateral sclerosis. Neural Regen Res 16:1723-1729.

Yang ZY, Zhou L, Meng Q, Shi H, Li YH (2020) An appropriate level of autophagy reduces emulsified isoflurane-induced apoptosis in fetal neural stem cells. Neural Regen Res 15:2278-2285.

Zhang J, Liang H, Zhu L, Gan W, Tang C, Li J, Xu R (2018a) Expression and distribution of arylsulfatase B are closely associated with neuron death in SOD1 G93A transgenic mice. Mol Neurobiol 55:1323-1337.

Zhang J, Huang P, Wu C, Liang H, Li Y, Zhu L, Lu Y, Tang C, Xu R (2018b) Preliminary observation about alteration of proteins and their potential functions in spinal cord of SOD1 G93A transgenic mice. Int J Biol Sci 14:1306-1320.

Zhang W, Benmohamed R, Arvanites AC, Morimoto RI, Ferrante RJ, Kirsch DR, Silverman RB (2012) Cyclohexane 1,3-diones and their inhibition of mutant SOD1-dependent protein aggregation and toxicity in PC12 cells. Bioorg Med Chem 20:1029-1045.

Zhang YJ, Jansen-West K, Xu YF, Gendron TF, Bieniek KF, Lin WL, Sasaguri H, Caulfield T, Hubbard J, Daughrity L, Chew J, Belzil VV, Prudencio M, Stankowski JN, Castanedes-Casey M, Whitelaw E, Ash PE, DeTure M, Rademakers R, Boylan KB, et al. (2014) Aggregation-prone c9FTD/ALS poly(GA) RAN-translated proteins cause neurotoxicity by inducing ER stress. Acta Neuropathol 128:505-524.

Zhou Y, Lu Y, Fang X, Zhang J, Li J, Li S, Deng X, Yu Y, Xu R (2015) An astrocyte regenerative response from vimentin-containing cells in the spinal cord of amyotrophic lateral sclerosis's disease-like transgenic (G93A SOD1) mice. Neurodegener Dis 15:1-12.

C-Editor: Zhao M; S-Editors: Yu J, Li CH; L-Editors: Yu J, Song LP; T-Editor: Jia Y